The impact of Land Use Land Cover (LULC) changes on Land Surface Temperature (LST); a case study of Addis Ababa City, Ethiopia

Daniel Muange Mbithi [1] **, Ermias T. Demessie** [2] **, Tendai Kashiri** [2]

Kenya Meteorological Services, Laikipia Airbase,
P.O. Box 192-10400 Nanyuki Town, Kenya

Abstract

Urbanization has been a major force of Land Use Land Cover (LULC) throughout human history that has had a great impact on climate change. To evaluate the effects of atmospheric correction, Normalized Difference Vegetation Index (NDVI) was calculated from both the original image and atmospherically corrected image and to derive the emissivity image, the NDVI equation was written in the spatial modeler of ERDAS.

This study examined LULC changes in the capital of Ethiopia, Addis Ababa from 1986 to 2010. Urban/built-up areas expanded dramatically, while agricultural land and forest declined. Barren land increased, mainly in the boundary areas between forest and dry agricultural fields especially in steeply sloping areas. The observed changes in LULC were largely attributed to population pressure on the land, a rapidly growing infrastructure and poor land use planning. Changes in LULC were accompanied by changes in Land Surface Temperature (LST) leading to an intensified Urban Heat Island (UHI) effect in the urban areas. The abundance of forest was an important factor influencing LST.

Moreover, temperature differences between the urban/built-up and the surrounding rural areas significantly widened. The study assessed the UHI spatial patterns and temporal variations in the Addis Ababa city. The urban-rural temperature differences between the urban core and its surrounding areas showed a maximum difference of more than 20°C. Greening of the urban set up was highly recommended in this study.

1. Introduction

Changes in land use land cover (LULC) affect the underlying biotic diversity, actual and potential primary productivity, soil quality, runoff, and sedimentation rates, the dynamics of which cannot be well understood without knowledge of the land use/cover change that drives them. LULC changes is one of the most visible results of human's modification of the terrestrial ecosystem, and it has a significant impact on the local, regional, and global environment, Weng et al (2001). Urbanization has been a major force of LULC throughout human history that has had a great impact on climate change (CC). Covered with buildings, roads, and other impervious surfaces, urban areas generally have higher absorption of solar radiation and greater thermal capacity and conductivity, leading to a relatively higher temperature in the urban areas compared with the surrounding rural areas.

Land surface temperature (LST), which is controlled by the surface energy balance, atmospheric state and thermal properties of the surface/subsurface rocks, is one of the important parameters in several environmental models, Becker and Li (1990). LST is important for environmental studies and management of the Earth's resources because it determines the effective radiating temperature of the Earth's surface. It is also a major factor in determining the partition of the available energy into sensible and latent heat fluxes. For example, the rate of change of LST is sensitive to the characteristics of the land surface such as soil moisture, land use and vegetation, Gillies et al (1997); Verstraeten et al (2006).

Previous studies have demonstrated that the LST product retrieved from thermal infrared (TIR) sensors can be used to monitor the urban heat island (UHI) effect. For example, Pongracz et al

(2006) used day- and night-time surface temperature time series observed by MODIS to determine UHI intensities over the ten most populated cities of Hungary. Spatial structures of UHIs were determined and compared for different seasons and macro-circulation conditions. Hung et al (2006) analyzed the UHI in 18 Asian mega cities using cloud free, day and night Terra MODIS LST products acquired between 2001 and 2003. Spatial pattern of UHIs for each city were examined over its diurnal cycle and seasonal variations. They found that both the magnitude and extent of UHIs were highly positively correlated to population size of the cities, indicating the significant impacts of urban growth on the UHI problems in Asia.

2. Data and Methodology

2.1 Data collection

The study used topographic map of the area at a scale of 1:250,000 dated 1984 and Landsat images of years 1986 (TM) and 2010 (TM). Scenes were required to be of the same phenological cycle (dry or wet season) and have little or no cloud cover. All Landsat images were accessed free of charge from U.S. Geological Survey (USGS) Center for Earth Resources Observation and Science (EROS) via http://glovis.usgs.gov/. All scenes supplied by the EROS Data Center had already been georeferenced to the Universal Transverse Mercator (UTM) map projection (Zone 37), WGS 84 datum and ellipsoid.

Several preprocessing methods were implemented before the classification and the change detection. These include geometric correction, radiometric correction, atmospheric correction, topographic normalization and temporal normalization.

2.2 Atmospheric correction

Atmospheric correction methods account for one or more of the distorting effects of the atmosphere and thereby convert the brightness values of each pixel to actual reflectances as they would have been measured on the ground. The FLAASH atmospheric correction algorithm was used to convert the at-sensor spectral radiance to reflectance at the surface of the Earth. To eliminate the effects of atmospheric scattering and absorption in the image and to increase the accuracy of surface type classification, the original DN values were converted to surface reflectance by using FLAASH atmospheric Correction. This procedure is divided into two stages:

(1) Converting DN values to spectral radiance and

(2) Transferring the sensor detected radiance into surface reflectance.

To evaluate the effects of atmospheric correction, NDVI was calculated from both the original image and atmospherically corrected image by using the following formula:

$$\text{NDVI} = \frac{\rho_4 - \rho_3}{\rho_4 + \rho_3} \quad \text{……………………………………………………………………………… (1)}$$

In previous studies, NDVI was commonly used to evaluate the effects of atmospheric correction process. The results shown in Figure 2 and Table 1 indicated that the NDVI of the surface reflectance is greater than that of the original values. Thus, quality of the image was improved after eliminating the negative effects of molecular scattering, gaseous observation, and aerosols. Vermote et al (2002) also reported that the NDVI values, on average, increased from -0.26 to 0.10 after atmospheric corrections.

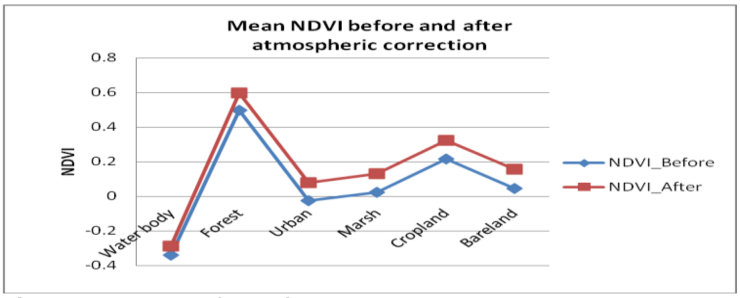

***Figure 2*: Mean NDVI for each LULC**

Water body		Forest		Urban		Marsh		Cropland		Bare land	
NDVI_b	*NDVI_a*	*NDVI_b*	*NDVI_a*	*NDVI_b*	*NDVI_a*	*NDVI_b*	*NDVI_a*	*NDVI_b*	*NDVI_a*	*NDVI_b*	*NDVI_a*
-0.36	-0.315	0.482	0.582	-0.02	0.079	0.02	0.128	0.25	0.356	0.04	0.152
-0.33	-0.282	0.465	0.566	-0.035	0.066	0.04	0.143	0.189	0.296	0.058	0.165
-0.32	-0.267	0.511	0.608	-0.03	0.073	0.013	0.116	0.224	0.332	0.02	0.134
-0.346	-0.296	0.533	0.629	-0.012	0.089	0.02	0.131	0.204	0.311	0.06	0.169
-0.339	**-0.29**	**0.49775**	**0.5963**	**-0.0243**	**0.07675**	**0.02325**	**0.1295**	**0.21675**	**0.32375**	**0.0445**	**0.155**

***Table 1*: NDVI for each LULC before (*NDVI_b*) and after (*NDVI_a*) atmospheric correction**

2.3 Temporal Normalization

An additional step (temporal normalization) was required to completely remove non-surface noise and improve temporal homogeneity of satellite imagery. Therefore 8 reservoir sites and 5 bare sites were used to normalize the 1986 TM image (slave) with respect to 2010 TM image (reference). The resulting normalization equation is shown in Table 2.

	Regression models	r^2	Normalization targets
2010 TM B2	=-25.2 + 1.03 (1986 TM B2)	0.981	8 wet and 4 dry
2010 TM B3	=-26.4 + 1.03 (1986 TM B3)	0.993	6 wet and 5 dry
2010 TM B4	=-21.7 + 0.98 (1986 TM B4)	0.987	5 wet and 5 dry

***Table 2*: Image normalization regression models developed**

3. Result and Discussion

3.1 Land use and land cover changes

A hierarchical class grouping was adopted to label and identify the classes in both images. First, the unsupervised ISODATA clustering was used. 25 initial classes were found and then after a rigorous identification and labeling process the original 25 classes were progressively reduced to 10 and 6 classes.

Table 3 lists the initial state classes in the columns, the final state classes in the rows and the unchanged areas in the diagonal cells. For each initial state class (i.e., each column), the table indicates how these pixels were classified in the final state image. A total of 48.65 km^2 was classified as Urban in the initial state image (1986), while 154.15 km^2 was classified as Urban in the final state image (2010). 105.5 km^2 urban land cover increased over the 24 years studied.

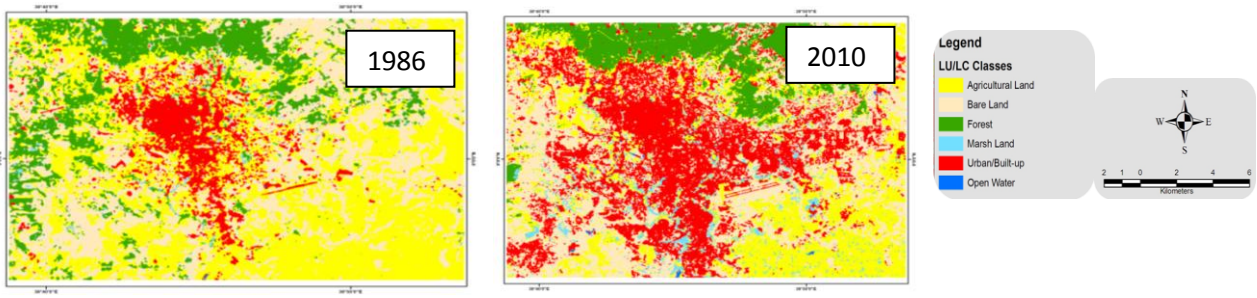

***Figure 3*: LULC in 1986 and 2010**

In the initial state (1986) image, 236.88km^2 of land was classified as Agricultural land, but only 129.93 km^2 of land was classified as Agricultural land in the final state image. This means a total of 106.99 km^2 of seasonal wetlands with low moisture were lost and/or converted to another land cover/use type during the period 1986 to 2010 (Table 3). Similarly a reduction in Forest land cover by 22.15 km^2 was also observed. Out of the 154.15 km^2 of urban class in the final state image, 60.17 km^2 (39%) has come from agricultural land use.

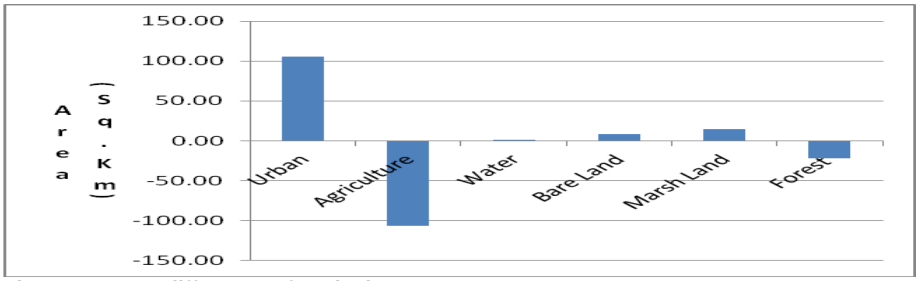

***Figure 4*: Image difference of each class**

		Initial State Image (1986)						
		Urban	Agriculture	Water	Bare Land	Marsh Land	Forest	Class Total
Final State Image (2010)	Urban	41.42	60.17	0.02	45.55	1.13	5.86	154.15
	Agriculture	0.77	90.72	0.00	19.27	1.14	18.02	129.93
	Water	0.15	0.75	0.06	0.18	0.00	0.07	1.21
	Bare Land	5.83	67.91	0.00	103.62	1.97	17.28	196.60
	Marsh Land	0.38	10.75	0.00	5.87	1.48	2.36	20.84
	Forest	0.10	6.57	0.00	13.98	0.78	39.52	60.96
	Class Total	48.65	236.88	0.08	188.46	6.50	83.11	
	Class Changes	7.23	146.16	0.02	84.85	5.03	43.59	
	Image Difference	105.50	-106.96	1.13	8.14	14.34	-22.15	

***Table 3*: Change detection statistics**

3.2 Changes in Land Surface Temperature (LST)

3.2.1 Land surface emissivity estimation

To obtain a reasonably high quality of LST, correction for surface emissivity is one of the major steps of correction process. Emissivity for ground objects from passive sensor data has been estimated using different techniques. Among those techniques are the normalized emissivity method, Gillespie, (1985), thermal spectral indices, Becker and Li, (1990), NDVI method, Van de Griend and Owe (1993), and classification-based estimation, Snyder et al (1998) among others.

According to Van de Griend and Owe's (1993) study, the relationship between emissivity and NDVI can be expressed by the following equation.

$$\varepsilon = 1.0094 + 0.047 \times \ln(NDVI). \quad \text{..... (2)}$$

The method that was used in this project is a slightly modified form of equation (2) to make the equation fit to the local condition of the study area.

$$\varepsilon(NDVI) = \begin{cases} 0.99, NDVI \le 0.01 \\ 1.0094 + 0.047 * \ln(NDVI), otherwise \end{cases} \quad \text{..... (3)}$$

To derive emissivity image the above equation was written in the spatial modeler of ERDAS as can be seen from the Figure below.

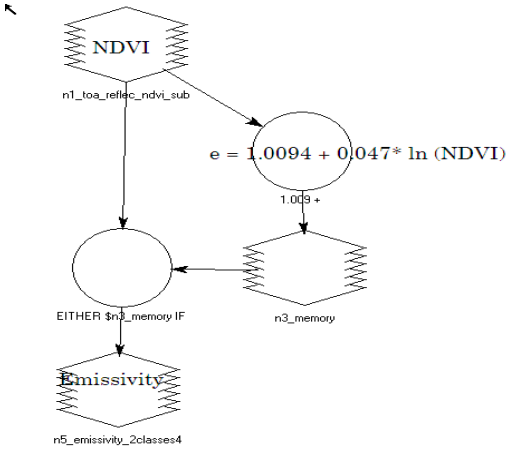

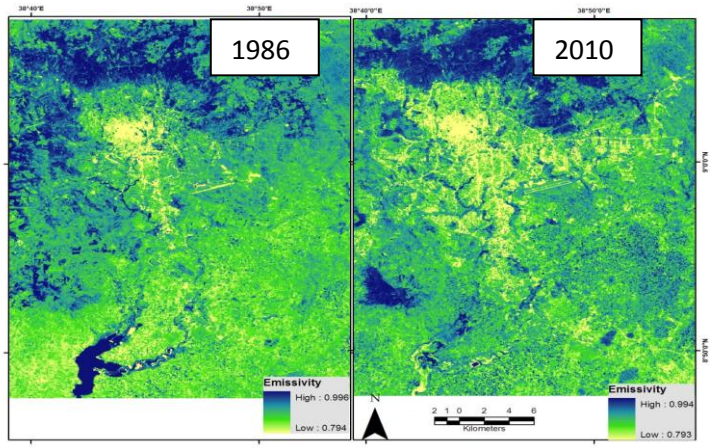

***Figure 5*: Emissivity retrieval in ERDAS Spatial Modeler** ***Figure 6*: Emissivity in 1986 and 2010**

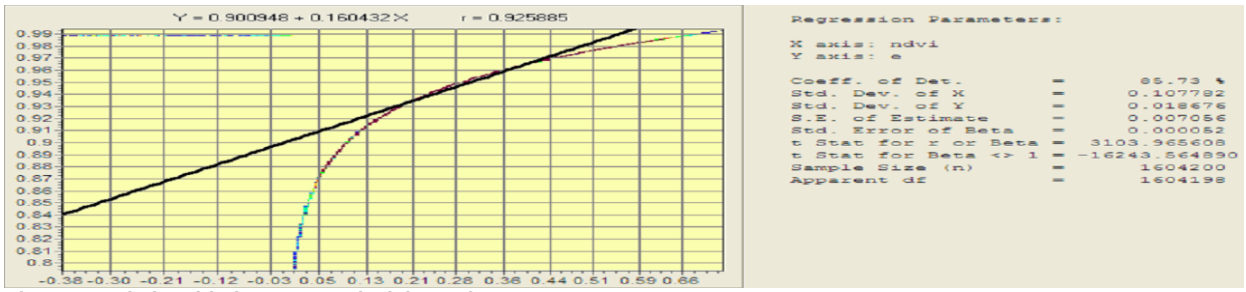

***Figure 7*: Relationship between Emissivity and NDVI**

3.2.2 Land Surface Temperature Retrieval

The satellite 'sees' only the radiation that emerges from the atmosphere, L_{sensor}, i.e., the radiance leaving the surface multiplied by transmissivity (τ), plus the radiance produced by the atmosphere. The radiance leaving the surface is a combination of the downwelling atmospheric radiance and the radiance produced by the surface of the Earth. Since the Earth is not a perfect blackbody, part of the downwelling radiance is reflected back. The radiance from the surface of the Earth is emissivity ε multiplied by blackbody radiation. The LST is obtained from the following expression of the RTE applied to the thermal infrared region:

$$L_{\text{sensor},\lambda} = \left[\varepsilon_\lambda B_\lambda(T_s) + (1-\varepsilon_\lambda)L^{\downarrow}_{\text{atm},\lambda}\right]\tau_\lambda + L^{\uparrow}_{\text{atm},\lambda} \quad \text{..... (4)}$$

where L_{sensor} is the at-sensor radiance or Top of Atmospheric (TOA) radiance, i.e., the radiance measured by the sensor, ε is the land surface emissivity, B_λ (Ts) is the blackbody radiance given by the Planck's law and Ts is the LST, $L_{atm}\downarrow$ is the downwelling atmospheric radiance, τ is the total atmospheric transmissivity between the surface and the sensor and $L_{atm}\uparrow$ is the upwelling atmospheric radiance. The main constraint of this method is that it needs in situ radiosounding launched simultaneously with the satellite passes.

The following Equation is Planck's equation relating spectral radiance and temperature.

$$L_\lambda = \frac{\varepsilon C_1 \lambda^{-5}}{\pi\left[\exp\left(\frac{C_2}{\lambda T}\right) - 1\right]} \qquad T = \frac{C_2}{\lambda \ln\left(\left[\frac{\varepsilon C_1 \lambda^{-5}}{\pi L_\lambda}\right] + 1\right)} \quad \text{..... (5)}$$

where $C_1 = 3{\cdot}742 \times 10^{-16}\ \text{W m}^2$, $C_2 = 0{\cdot}0144\ \text{m K}$, λ = wavelength in m, ε = emissivity

Equation (3) can also be written as follows:

$$LST = \frac{K_2}{\ln\left(\frac{\varepsilon * K_1}{L_\lambda} + 1\right)} \quad \text{..... (6)}$$

Constant	K1	K2
Units	W/(m² sr μm)	Kelvin
L4 TM	671.62	1284.30
L5 TM	607.76	1260.56
L7 ETM+	666.09	1282.71

The at-sensor brightness temperature assumes that the Earth's surface is a black body, and includes atmospheric effects (absorption and emissions along path). These temperature values do not account for the different land cover types. In order to determine an actual surface temperature it is necessary to know the surface material and from this determine its emissivity value. The inclusion of the emissivity to calculate the actual surface temperature does not change the pattern of temperatures for each land cover class, but it does act to accentuate the differences.

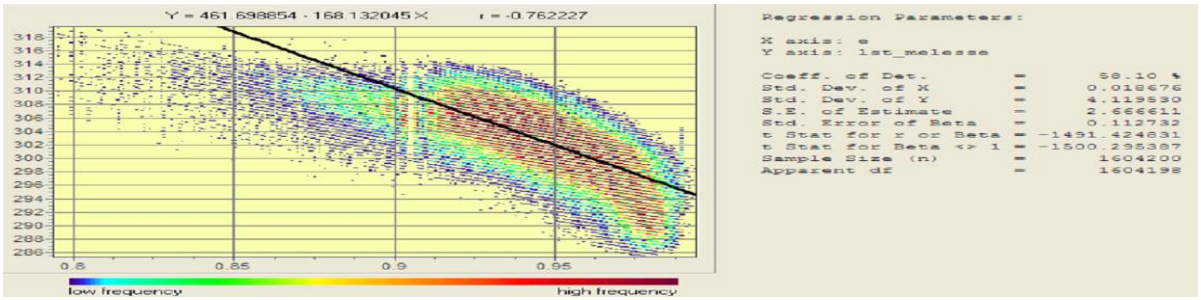

***Figure 8*: Relationship between LST and Emissivity**

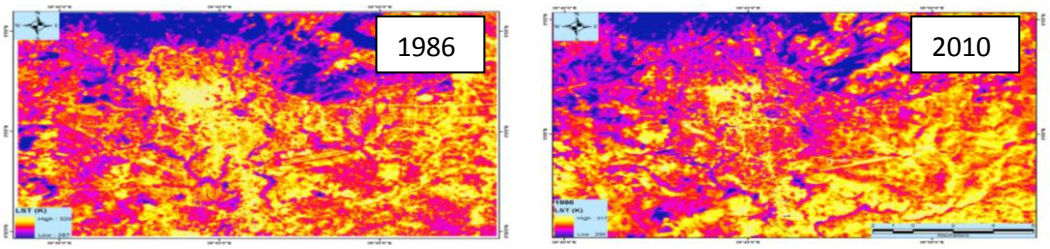

***Figure 9*: LST map in 1986 (upper position) and 2010 (lower position)**

3.3 The impact of land use change on LST

The changes in LULC resulted in changes in LST, especially in the urban areas. Since 1986, many urban areas expanded dramatically (Fig. 9). The increased temperature in the urban areas was mainly a reflection of rapid urban expansion during the 24-year period. In addition to urban expansion, there have been significant changes to the old parts of the cities. A great amount of land in those parts has been re-developed by the government or private companies for the purpose of construction new residential, shopping, and industrial facilities. The conversion of forest and agricultural land into urban/built-up land also contributed to the increased LST. The new houses, along with supporting infrastructures, were frequently located in high-quality agricultural land or forestland, while old factories were abandoned and the land remained unused afterward. This relocation reduced agricultural area and increased LST. In the past, agricultural or forest areas could provide a buffer zone between the urban and rural areas to absorb excess heat generated by automobiles and factories. From Figure 9 it can be seen clearly that vegetation has great impact on reducing land surface temperature.

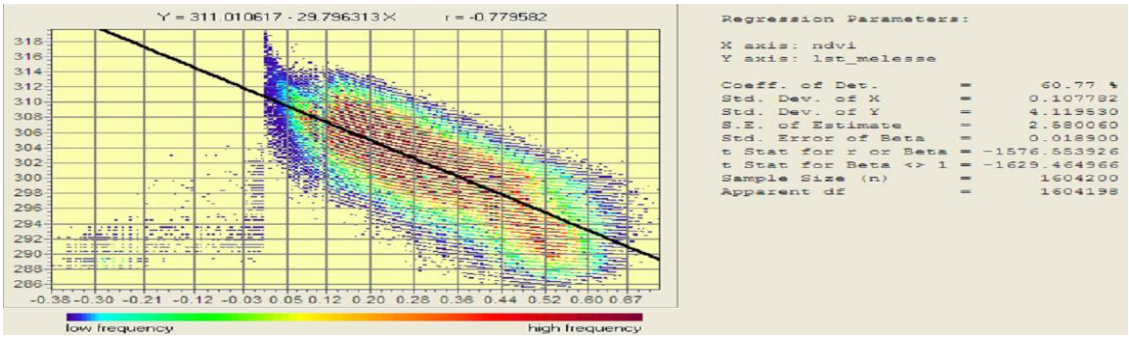

***Figure 10*: Relationship between LST and NDVI**

NDVI has been widely used as an indicator of vegetation abundance to estimate LST in studies of urban heat islands. In this study, NDVI and LST were found to be closely correlated. The correlation coefficient reached as high as 0.78 (Figure 10). Therefore, the impact of LULC on LST may be examined by an analysis of the changes in NDVI.

Figure 11 show a temperature difference between the urban center and its surrounding areas of a maximum of 15 ℃. The land surface temperature in the urban center was a mean of 5℃ warmer than that in surrounding rural areas. The results show that UHIs existed significantly in the city of Addis Ababa.

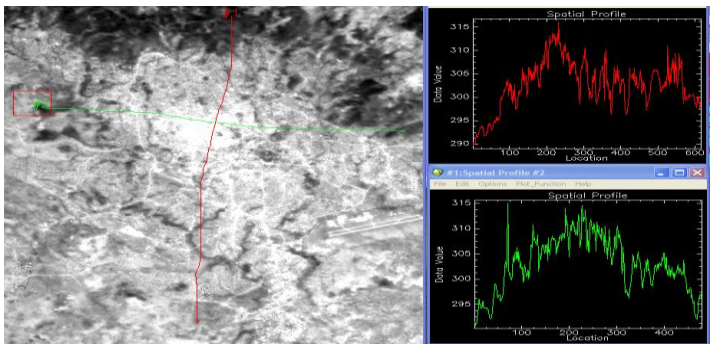

***Figure 11*: LST difference between urban and rural areas**

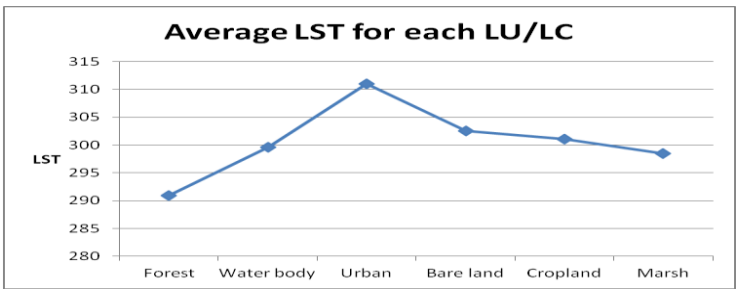

***Figure 12*: Average LST for each LU/LC**

4. Conclusion and Recommendation

This study has examined LULC changes in the capital of Ethiopia, Addis Ababa from 1986 to 2010. The results indicated that urban/built-up areas expanded dramatically, while agricultural and forest land declined. Barren land increased, mainly in the boundary areas between forest and dry agricultural fields, especially in steeply sloping areas. The observed changes in LULC were largely attributed to population pressure on the land, a rapidly growing infrastructure and poor land use planning. Changes in LULC were accompanied by changes in LST. Moreover, temperature differences between the urban/built-up and the surrounding rural areas significantly widened. The study assessed the UHI spatial patterns and temporal variations in the Addis Ababa city. The urban-rural temperature differences between the urban core and its surrounding areas show a maximum difference of 15℃. This could lead to an intensified urban heat island effect in the urban areas. The abundance of forest was an important factor influencing LST.

References

Becker, F. and Li, Z., (1990): Temperature independent spectral indices in thermal infrared bands; Rem. Sens. Environ. , 32, 17–33.

Gillespie A, Rokugawa S, Matsuna G T, Cothern J S, Hook S and Kahle, A. B. , (1998): A temperature and emissivity separation algorithm for Advanced Space- borne Thermal Emission and Reflection Radiometer (ASTER) images; IEEE Trans. Geosci. & Rem. Sens. 36 1113–1126.

Gillies, R.R., Carlson, T.N., Cui, J., Kustas, W.P. and Humes, K.S. , (1997): A verification of the 'triangle' method for obtaining surface soil water content and energy fluxes from remote measurements of the Normalized Difference Vegetation Index (NDVI) and surface radiant temperature. International Journal of Remote Sensing, 18 (15): 3145-3166.

Hung, T., Uchihama, D., Ochi, S. and Yasuoka, Y., (2006): Assessment with satellite data of the urban heat island effects in Asian mega cities. International Journal of Applied Earth Observation and Geoinformation, 8(1): 34-48.

Pongrácz, R., Bartholy, J., Dezső, Zs., (2006): Remotely sensed thermal information applied to urban climate analysis. Advances in Space Research, 37, 2191-2196.

Snyder, W. C, Wan. Z, Zhang Y and Feng Y-Z. , 1998: Classification-based emissivity for land surface temper- ature measurement from space; Int. J. Rem. Sens. 19 2753–2774.

Van de Griend, A. A and Owe M., (1993): On the relationship between thermal emissivity and the normalized difference vegetation index for natural surfaces; Int. J. Rem. Sens. 14 1119–1131.

Vermote E. F.; El Saleous, N.Z and Justice, C. O., (2002): Atmospheric correction of MODIS data in the visible to middle infrared: first results. Remote Sensing of Environment, 83, 97-111.

Verstraeten, W.W., Veroustraete, F., van der Sande, C.J., Grootaers, I. and Feyen, J., (2006): Soil moisture retrieval using thermal inertia, determined with visible and thermal spaceborne data, validated for European forests. Remote Sensing of Environment, 101(3): 299-314.

Weng, Q., Lo, sand C.P., (2001): Spatial analysis of urban growth impacts on vegetative greenness with Landsat TM data. Geocarto International, 16 (4), 17–25.